Case Studies in Thermal Engineering 41 (2023) 102562

Contents lists available at ScienceDirect

Case Studies in Thermal Engineering

journal homepage: www.elsevier.com/locate/csite

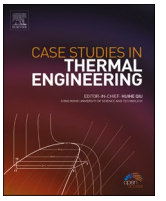

Photo-thermo-mechanical model for laser hair removal simulation using multiphysics coupling of light transport, heat transfer, and mechanical deformation (case study)

Vannakorn Mongkol, Wutipong Preechaphonkul, Phadungsak Rattanadecho *

Center of Excellence in Electromagnetic Energy Utilization in Engineering CEEE, Department of Mechanical Engineering, Faculty of Engineering, Thammasat University, Khlong Luang, Pathum Thani, 12120, Thailand

ARTICLE INFO

Keywords:
Laser hair removal
Light transport
Bioheat
Mechanical deformation
Photo-thermo-mechanical model
Numerical simulation

ABSTRACT

The mathematical model has become one of the tools for prediction to assist physicians and specialists with hair laser removal in dermatology. This paper proposes a model that comprehensively predicts optical, thermal, and mechanical responses within the skin during laser hair removal to determine optimal therapeutic conditions and prevent skin tissue damage. This research highlighted developing a mathematical model using multiple physics of light transport, heat transfer, and mechanical deformation. The present mathematical model is resolved using the 2D axisymmetric finite element method (FEM) with optical, thermal, and mechanical properties to characterize the laser intensity, temperature distribution, mechanical stress, and displacements within skin tissue. The comparison of the simulated results in laser wavelengths of 595 nm, 800 nm, and 1064 nm is also provided. The results revealed that laser deposition with skin tissue depends on the wavelength and optical diffusion coefficient. Applying the 1064 nm performs the best treatment outcome for hair laser removal. In contrast, 595 nm and 800 nm might lead to adverse pain sensations. The high temperature caused an increase in mechanical stress and displacement. The results of this study indicate that laser therapy has certain limitations that must be considered.

1. Introduction

Recently, laser has caught the attention of researchers, utilizing it in medical treatments such as dermatology [1]. Laser hair removal is one of the medical applications. It is a medical process that employs intense light and pulses to permanently eliminate hair from the armpits, legs, shins, face, and even private parts [2]. Hair follicles have a high melanin content filled with stem cells capable of repairing the hair follicle, and hair is the primary target tissue. The hair follicle can be destroyed and entirely removed at a temperature of 65 °C [3,4]. The destruction of hair follicles depends on several factors, such as suitable wavelength, pulse size, and intensity [5]. When skin and targeted tissue receive laser irradiation, the energy from the laser will be absorbed and produce heat within the tissue. Healthy tissue in the surrounding area may experience undesired heating, leading to thermal damage and pain during laser hair removal. The research found that negative sensations and emotional experiences cause pain [6]. Human skin tissues respond to thermal, mechanical, and chemical stimuli with thermal and mechanical sensitivity of 43 °C and 0.2 MPa, respectively [7]. Hence, it is necessary to govern and decrease heat transfer inside the targeted tissue, leading to damage prevention of surrounding tissues.

* Corresponding author.
E-mail address: ratphadu@engr.tu.ac.th (P. Rattanadecho).

https://doi.org/10.1016/j.csite.2022.102562
Received 3 August 2022; Received in revised form 9 October 2022; Accepted 13 November 2022
Available online 25 November 2022

Physicians and researchers have been studying physiological phenomena inside human skin for tissue damage prevention while removing hair with laser therapy, producing and developing more efficient and safer equipment [8].

Several researchers have studied laser treatments for hair removal, e.g., Goldberg et al. [10] investigated the efficacy of hair removal on various body parts using a laser at different intensities and discovered that the size of the laser intensity affects the regeneration of hair. There are other experimental studies also included animal testing [9,11–15] In recent years have seen an increase in the use of mathematical models due to their benefits, which include cost savings, shorter study times, the ability to define a broad range of treatment conditions, Etc. Researchers have presented mathematical models for laser hair removal. In 2009, Sun et al. [15] proposed a Fourier model to predict temperature profiles of human skin for laser hair removal, which considers optical properties of melanin, water, and blood in the human skin. It was discovered that the average temperature of hair follicles rises as a linear function of fluence. Additionally, there are studies of thermal damage investigation for unwanted heat prevention using mathematical models for laser hair removal, which indicate that applying a small spot size and fluence, including using a long pulse duration, can reduce thermal damage area [16,17]. In 2014, Kim and Lee proposed a mathematical model that studied the effect of color skin types on temperature profiles for laser hair removal and found that dark skin can lead to more adverse effects [18]. In 2019, a 3D human skin model was proposed by Mármol and Villena [19] to evaluate the safety and efficacy of laser wavelengths and cooling devices for laser hair removal treatment and thermal injury prevention. In addition, there are many related studies [20–27] on the development of mathematical models using laser therapy, such as the study of phase change effect on temperature [24], tumor ablation [20,21], and increasing the efficiency of light absorption through nanoparticle injection [26,27], as well as the cooling effect of blood circulation in blood vessel embedded in the skin [22,23]. Most simulation studies of laser treatment in dermatology and previously mentioned works widely used the non-Fourier model of Pennes's bioheat equation in the mathematical model, induced by Pennes [28], for solving heat problems in bio-material [16–27,29–36].

In addition, when skin tissue is exposed to high temperatures during thermotherapy induced by laser, mechanical stress occurs within the skin tissue due to thermal denaturation, resulting in the deformation of the skin [37]. Moreover, thermal and mechanical energy converts to ionic current, resulting in the sensation of physical pain during therapeutic [38]. Few researchers have presented models to investigate mechanical response of human skin due to thermal effects. Jor et al. [39] developed a 3D discrete fiber skin model and discovered that the deformation was related to density, fiber thickness, and tissue stiffness. Garaizar et al. [40] developed a model to investigate the mechanical effects of the skin from the thermal and external load. Moreover, Larrabee [41] proposed a model to study the human skin's mechanical and viscoelastic properties. The viscoelastic properties permit better movement of skin structures without rupturing compared to elastic properties, which protect against injury of skin tissue. Recently, In previously published work, Wongchadakul et al. [25] presented the 2D asymmetric model of human skin to study the influence of wavelength, intensities, and irradiation time on the human skin's mechanical response during laser treatment. Furthermore, some studies study the mechanical stain from thermal effects in biological tissues as well, such as breast and liver cancer [34,42].

From literature exploration, we observed that in the past research on mathematical modeling of laser hair removal and other laser therapy, Beer-Lambert's law is used to calculate laser deposition within skin tissue since it is simple to apply and avoids increasing the complexity of the mathematical model [16–18,21,25–27]. Nevertheless, the optical diffusion coefficient, one of the essential parameters of light diffusion in the medium that must be calculated systematically, is required. For a comprehensive analysis, laser energy deposition within dermal tissue has to be analyzed using the light transport equation, which has been used in previous studies [14,19,43–45]. In another observation, previous research concentrated on modeling for studying thermal behavior from the effects of wavelengths, beam diameters, and laser intensities. In contrast, investigating the mechanical phenomenon of the skin of laser hair removal remains challenging as evidence has shown that there are few studies have examined the mechanical effects, e.g., thermal stress and skin displacement, another critical factor that might directly affect pain sensation during laser hair removal and other therapy. Further, we observed that there are a few research that proposes a mathematical model using Multiphysics of the light transport equation, heat transfer, and mechanical deformation for laser hair removal.

Therefore, this present study employs a photo-thermo-mechanical model to predict the thermal and mechanical response of laser hair removal. The current model is one of the few mathematical modelings of laser hair removal using multiple physics of light transport, bioheat transfer, and mechanical deformation and is developed based on a 2D axisymmetric model. The model utilized the laser deposition energy described by the light transport equation instead of Beer-Lambert's law, and Pennes's bioheat equation describes the transient temperature of skin tissue. In addition, the equilibrium equation is used to analyze the mechanical deformation within tissue. Within the context of this model, numerical research was conducted to investigate the impact that wavelengths have on the laser intensity, temperature distribution, Von-Mises stress, and total displacement in the skin. Therefore in the study, the numerical simulation results mentioned above were compared. The findings of this study can be used to enhance the phenomena that must be considered for adequate therapy preparation and therapeutic outcomes and to be a sample for further development in other related mathematical modeling work.

2. Problem description

Laser hair removal is the chosen method for physicians and aesthetic specialists for hair removal on various parts of the human body. The outer layer of the skin is irradiated with a laser to heat it to its hair-eliminating temperature. The negative aspect of using laser techniques for hair removal is the undesired heat to surrounding tissue, which may cause thermal injury to healthy tissue and pain during therapy. However, there are two primary pain sensations: thermal and mechanical. The high temperature and mechanical stress within skin tissue might also have adverse effects. A comprehensive investigation of thermal and mechanical phenomena is still challenging for appropriate therapeutic preparation. Consequently, we presented the photo-thermo-mechanical model. The proposed

model was utilized to examine the temperature distribution, Von-Mises stress, and total skin displacement during laser hair removal.

3. Method and model

The focus of the study was on the thermal and mechanical responses of skin and hair during laser hair removal. Laser energy calculation is the first step in understanding laser deposition within skin tissue. Then, the light energy absorbed, which led to an increase in temperature and was related to mechanical deformation phenomena in skin tissue, was examined. For the modeling, the model is created under a two-dimensional (2D) axisymmetric in a cylindrical coordinate system for mathematical modeling. The mathematical model considers the light transport, heat transfer, and mechanical deformation in skin tissue using the COMSOL Multiphysics software based on the Finite Element Method (FEM). The light transport equation, Pennes's bioheat equation, and the equilibrium equation are used to calculate the deposition of laser light, heat transfer, and mechanical deformation within skin tissue. Pennes's bioheat equation analyzes the heat diffusion within the skin tissue. We used wavelengths of 595 nm, 800 nm, and 1064 nm for providing the temperature, Von Mises stress, and skin displacement. The model properties were referred to in the literature [12–15,18,25,46–56] and shown in Table 1.

3.1. Physical model for numerical analysis

According to the biological structure of human skin, skin tissue contains several organs. In this study, the structure of the skin has been simplified. The photo-thermo-mechanical model consists of multilayers of the epidermis, dermis, hair, and hair follicles. Fig. 1 shows a 2D axisymmetric skin model and details obtained from the literature [14,49,50]. Moreover, this model considers the effect of light reflection on the skin surface. The light transport equation describes the laser deposition with skin tissue as the effect of light absorption and scattering. All properties are taken directly from the literature [12–15,18,25,46–56].

For problem simplification, the following assumptions have been made:

1. The model is considered in the two dimensions of axisymmetric analysis.
2. The material properties of skin tissues are assumed to be isotropic and homogeneous.
3. The interfaces between tissues are considered to be smooth interfaces.
4. Phase change and chemical reactions within skin tissues are ignored.

3.2. Equation for light transport analysis

Light transport is considered in all domains and is described by the following differential equation [44]:

$$\frac{\partial}{\partial t}\varnothing - D\nabla^2\varnothing + c_{e,d,h}\mu_a\varnothing = 0 \tag{1}$$

$$D = c_{e,d,h}[3(\mu_a + (1-g)\mu_s)]^{-1} \tag{2}$$

Where $\varnothing$ is the intensities of laser (W/m^2), D is the optical diffusion coefficient (m^2/s) of skin tissue, $c_{e,d,h}$ is the speed of light in the epidermis, dermis or hair, μ_a is the absorption coefficient (1/m) of skin, μ_s is the scattering coefficient (1/m) and g is the optical anisotropy factor.

Table 1
Thermal, mechanical and optical properties using in this study [12–15,18,25,46–56].

	Epidermis	Dermis	Hair
Tissue density, ρ (kg /m^3)	1200	1090	1030
Specific heat of tissue, C (J/(Kg K))	3950	3350	3582
Thermal conductivity, k (W/(m K))	0.24	0.42	0.558
Blood perfusion, ω_b (1/s)	–	0.0031	–
Metabolic heat generation, Q_{met} (W/m^3)	368	368	368
Thermal expansion coefficient, α (1/ K)	0.0001	0.0001	0.0001
Poisson's ratio (–)	0.48	0.48	0.48
Young's modulus (GPa)	0.102	0.0102	4.1
Absorption coefficient, μ_a (1/m), 595 nm	1708.49	85.42	6000
Absorption coefficient, μ_a (1/m), 800 nm	858	24	3800
Absorption coefficient, μ_a (1/m), 1064 nm	226.03	11.30	2500
Scattering coefficient, μ_s (1/m), 595 nm	24243.70	24243.70	3844.86
Scattering coefficient, μ_s (1/m), 800 nm	18031.25	18031.25	1421.08
Scattering coefficient, μ_s (1/m), 1064 nm	13557.33	13557.33	544.79
Anisotropy, g, 595 nm	0.9	0.79	0.9
Anisotropy, g, 800 nm	0.85	0.85	0.9
Anisotropy, g, 1064 nm	0.85	0.85	0.9
Refractive index, n	1.37	1.37	1.37
Ratio of reflected light, 595 nm	0.45	–	–
Ratio of reflected light, 800 nm	0.6	–	–
Ratio of reflected light, 1064 nm	0.5	–	–

3.2.1. Boundary conditions for light transport analysis

On the skin surface, it assumed that laser continually and uniformly exposure irradiation along the boundary conditions [44] as shown in Fig. 1

$$-\boldsymbol{n} \bullet (-D\nabla \varnothing) = (1-R)P(t)_{laser}c_0 \tag{3}$$

Where $P(t)_{laser}$ is the laser irradiance at the upper surface (W/m^2), c_0 is speed of light in vacuum and R is the ratio of reflected light.

The lower and outer surface were assumed that laser flux continuous boundary condition.

$$-\boldsymbol{n} \bullet (-D\nabla \varnothing) = 0 \tag{4}$$

3.3. Equations for heat transfer analysis

Pennes's bioheat is considered in all domains to analyze heat transfer within each tissue [28].

$$\rho C\frac{\partial T}{\partial t} = \nabla \bullet (k\nabla T) + \rho_b C_b \omega_b (T_b - T) + Q_{met} + \mu_a \varnothing \tag{5}$$

Where ρ is tissue density (kg/ $/m^3$), C is tissue heat capacity (J/kg K), k is tissue heat conductivity ($W/m \bullet K$), T is tissue temperature ($^\circ C$), $\rho_b C_b \omega_b (T_b - T)$ is the blood perfusion term, T_b is the blood temperature (36 $^\circ C$) [25], ρ_b is the blood density (1060 kg/ m^3) [25], C_b is the specific heat capacity of the blood (3, 660 J/kg • K) [25], ω_b is the rate of blood perfusion ($1/s$), Q_{met} is Metabolic heat generation (W/m^3), and considering of term external heat sources of laser deposition (W/m^3).

3.3.1. Boundary condition for heat transfer analysis

The boundary conditions are specified in Fig. 1and the skin surface is under convection boundary conditions:

$$-\boldsymbol{n} \bullet (k\nabla T) = h_T(T_{air} - T) \tag{6}$$

Where T_{air} is the ambient temperature (20 °C) and h_T is heat transfer coefficient (10 $W/(m^2 \cdot K)$)

The internal interfaces between each tissue are a smooth condition which means no contact thermal resistance. So, it is assumed to be under a continuity boundary condition.

$$\boldsymbol{n} \bullet (k_u \nabla T_u - k_d \nabla T_d) = 0 \tag{7}$$

3.4. Equation for mechanical deformation analysis

As presented in previous studies [25,41,42], the model is simplified to a quasi-static model. The mechanical deformation such as displacements and stresses occurring within skin tissue that exposure laser light was investigated by using the equilibrium equations (equations (8a)-(8b), the stress-strain relationship (equation (9a)-(9c)), and the strain-displacement relationship (equation (10a)-(10b)) described in cylindrical coordinate systems [42].

$$\frac{\partial \sigma_{rr}}{\partial r} + \frac{\partial \sigma_{rz}}{\partial z} + \frac{\sigma_{rz} - \sigma_{\varnothing\varnothing}}{r} + F_r = \rho\frac{\partial^2 u_r}{\partial t^2} \tag{8a}$$

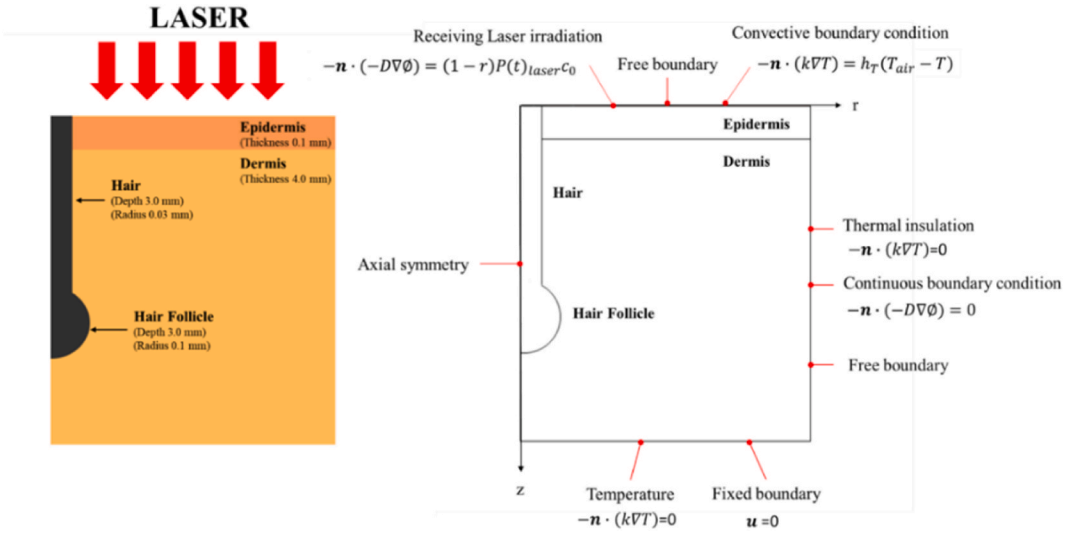

Fig. 1. Physical domain and boundary conditions.

$$\frac{\partial \sigma_{rz}}{\partial r}+\frac{\partial \sigma_{zz}}{\partial z}+\frac{\sigma_{rz}}{r}+F_z=\rho\frac{\partial^2 u_z}{\partial t^2} \tag{8b}$$

$$\varepsilon_{rr}=\frac{1}{E}[\sigma_{rr}-\nu(\sigma_{\varphi\varphi}+\sigma_{zz})]+\varepsilon^{th} \tag{9a}$$

$$\varepsilon_{zz}=\frac{1}{E}[\sigma_{zz}-\nu(\sigma_{\varphi\varphi}+\sigma_{rr})]+\varepsilon^{th} \tag{9b}$$

$$\varepsilon_{\varphi\varphi}=\frac{1}{E}[\sigma_{\varphi\varphi}-\nu(\sigma_{rr}+\sigma_{zz})]+\varepsilon^{th} \tag{9c}$$

$$\varepsilon_{rr}=\frac{\partial u_r}{\partial r},\varepsilon_{zz}=\frac{\partial u_z}{\partial z},\varepsilon_{\varphi\varphi}=\frac{u}{r}, \tag{10a}$$

$$\varepsilon_{rz}=\frac{1}{2}\left(\frac{\partial u_r}{\partial z}+\frac{\partial u_z}{\partial r}\right) \tag{10b}$$

$$\varepsilon^{th}=\int_{T_{ref}}^{T}\alpha dT \tag{11}$$

Where σ is the stress (Pa),ε is the strain, F is the external volumetric force (0 N/ m^3 for here), E is Young's modulus (Pa), ν is the Poisson's ratio and u is the displacement (m). ε^{th} is the thermal strain, α is the coefficient of thermal expansion (1/°C) and T_{ref} is 36 °C the reference temperature.

3.4.1. Boundary condition for mechanical deformation analysis

The bottom surface is fixed constraint boundary condition. The rest of boundary is considered free boundary condition and the initial stress and strain are set to zero:

$$\sigma_{ri},\sigma_{\varphi i},\sigma_{zi}\ and\ \sigma_{rzi}=0\ Pa \tag{12}$$

$$\varepsilon_{ri},\varepsilon_{\varphi i},\varepsilon_{zi}\ and\ \varepsilon_{rzi}=0 \tag{13}$$

3.5. Initial conditions

The initial value of light deposition is 0 W/m^2, the initial temperature is 36 °C (core body temperature), and initial displacement field is 0 mm.

3.6. Calculation procedure

To investigate the phenomenon within the tissue model during the hair laser removal process. FEM is used for solving numerical problems via COMSOL™ Multiphysics. The system of governing equations, boundary conditions, and initial values are systematically

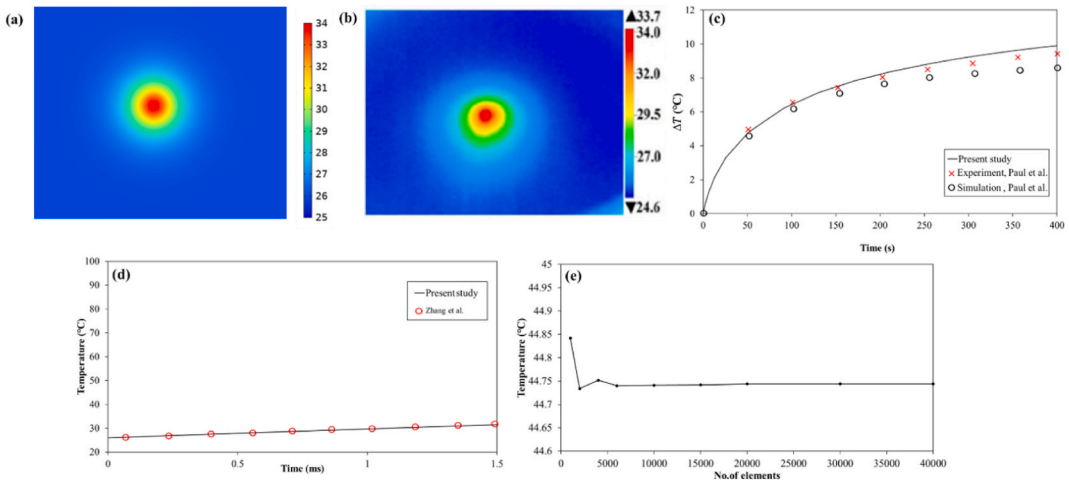

Fig. 2. (a) the present model results (top view), (b) Paul et al.'s experimental results [23], (c) validation results of present study against experimental results obtained by Paul et al. [23], (d) validation results of present study against numerical results obtained by Zhang et al. [44] (e) comparison between laser intensity profiles obtained from present study and obtained by Paul et al. [23], and (f) model's grid convergence curve.

calculated. The light transport equation, Pennes's bioheat, and equilibrium equation were applied in all domains. The initial and boundary conditions were followed in the previous section. The discretization of numerical models using triangular, edge, and vertex elements. In independent solving setting, initial and maximum time steps for solving of the transient problem were 1×10^{-3}, s and 0.1 s, respectively. The laser intensity within each tissue is obtained by calculating the light transport equation from laser irradiation and then used as input values in the bioheat equation to compute the heat source of laser deposition in each tissue, which raises the tissue temperature later. Simultaneously, the thermal strain was recalculated using the temperature distribution within skin tissue. Until 50 ms of irradiation, the laser's intensity, temperature, Von-Mises stress, and displacement are collected. In addition, the optimal number of elements that do not affect results changing for simulation is determined by a convergence test—testing with a wavelength of 1064 nm, power of laser 5 J/cm^2 at laser irradiation 50 ms, and properties taken from Table 1. As depicted in Fig. 2(f), the results of this convergence test revealed a grid of approximately 20,000 elements.

4. Validation of model

The experiment and simulation results obtained by the previously published work of Paul et al. [23] were used to investigate the accuracy of this present numerical model under identical testing conditions. In Paul's simulation, laser absorption energy is described by Beer-Lambert's law.In Paul et al.'s experiment, a tissue phantom (agar) was irradiated with a continuous-wave laser of 800 nm. The diameter and height of the tissues was 10 cm and 15 cm, respectively. The intensity of the incident laser beam on the tissue phantom is 32000 W/m^2, and the radius of the laser beam (σ) is 2.5 mm. The ambient temperature is 25 °C and considering convective heat transfer of 10 $W/(m^2 \cdot K)$). In this validation, The incident laser power is considered as a Gaussian distribution according to the following expression:

$$P_{laser} = P_0 \exp\left(-r^2 / 2\sigma^2\right) \tag{14}$$

The intensity of the incident laser beam on the tissue phantom (P_0) is 32000 W/m^2, and the radius of the laser beam (σ) is 2.5 mm [23]. The optical and physical properties of phantom tissue are in Table 2.

In addition, the numerical results obtained by Zhang et al. [44], similar work is also validated under the same conditions. The light transport equation is used in Zhang's model to calculate the laser energy within skin tissue in birthmark treatment by laser irradiation with fluence of 8 J/cm^2 of 1.5 ms of time irradiation. From the validation results as shown in Fig. 2(a–d) represents the surface temperature from (a) the present model, (b) Paul et al.'s experiment, (c) the comparison of temperature change over time between the present numerical results, experimental results, and simulation results obtained from Paul et al. [23], and (d) validation results of present study against numerical results obtained by Zhang et al. [44]. It shows great consistency with the contour temperature (a-b) and temperature data (c-d), a similar temperature profile trend. However, when the time irradiation reaches 200 s, the temperature difference between the present model and simulation results obtained from Paul et al. [23] was gradually increased until 400 s. Since the laser intensity profile is different, the numerical data obtained by Paul et al. [23] employs Beer-law Lambert's to calculate laser deposition, whereas the present study implements the light transport equation. It can be confirmed in Fig. 4(e), which displays the comparison between laser intensity profiles obtained from the present study and obtained by Paul et al. [23]. It indicates that the laser intensity calculated from the present study (Light transport equation) was deposited higher and could penetrate better than Paul et al. [23] (Beer-Lambert's law). Consequently, when irradiation continues, the difference in laser intensity deposited in phantom tissue directly affects temperature profiles. It still shows good agreement with Paul et al.'s experimental results [23] and provides credibility to the precision of the present numerical model.

5. Result and discussion

Naturally, when irradiating the skin with a laser, the two primary phenomena that occur in tissues are light absorption and heat generation. The laser light is absorbed by the tissue and converted to heat energy. Due to the unequal absorption coefficients and scattering, the amount of laser deposition in each tissue layer is different, directly resulting in treatment outcomes. Nevertheless, since skin tissue is a bio-elastic material, the mechanical deformation of thermal expansion could also occur. Consequently, the phenomenon of skin deformation during treatment must also be considered. During laser hair removal treatments, high temperatures can lead to thermal damage from undesired heat and mechanical deformation in the skin tissue arising in painful sensations. Controlling the heating and limiting the heated area is essential. Thus, comprehensive treatment outcome prediction of phenomena that possibly occur before the actual treatment assists physicians in improving safer and more effective therapeutic plans. In this section, the influence of wavelengths on temperature distribution and deformation of skin tissue during the laser hair removal treatment is investigated and illustrated.

Table 2
Properties of tissue phantom [23].

Properties	Phantom Tissue (agar)
Tissue density, ρ (kg/m^3)	1050
Specific heat of tissue, C (J/(Kg K))	4219
Thermal conductivity, k (W/(m K))	0.66
Absorption coefficient, μ_a (1/m)	530
Scattering coefficient, μ_s (1/ m)	40

5.1. Laser intensity distribution

Fig. 3(a–c) shows a 3D simulation of the laser intensity distribution within skin tissue layers and hair after 50 ms of laser irradiation with a laser fluence of 5 J/cm^2 of 595 nm, 800 nm, and 1064 nm. At all wavelengths, the laser intensity distribution can be clearly observed at the epidermis site. Even though the input of laser fluence is the same in all cases, the simulation reveals that 1064 nm laser deposits the most energy within skin tissue, followed by 800 nm and 595 nm, respectively. Fig. 7 (a), which depicts the laser intensity lines of 595 nm, 800 nm, and 1064 nm on the surface skin (r-axis and z = 0 mm), provides confirmation. The 1064 nm laser intensity line is the most intense at the skin's surface (epidermis layer). After skin tissue receives laser energy, all wavelengths decrease gradually along the longitudinal axis to the bottom of the skin. Fig. 7 (b) depicts the 595 nm, 800 nm, and 1064 nm laser intensity lines within hair tissue (z-axis and r = 0 mm). It indicates that 1064 nm laser energy can effectively reach the hair follicles. In contrast, the laser intensity lines of 595 nm and 800 nm are marginally distinct and less intense than those of 1064 nm. In comparison, 595 nm and 800 nm treatment performed poorly and was maintained at a low laser intensity level. Because the characteristics of the skin's light propagation and ability to penetrate vary with wavelength. It can be mathematically explained using the optical diffusion coefficient depicted in Fig. 4. It displays the comparison of the optical diffusion coefficient of skin tissues at 595 nm, 800 nm, and 1064 nm. The epidermis, dermis, and hair optical diffusion coefficients are clearly different. The highest optical diffusion coefficient in all tissues is 1064 nm, followed by 800 nm and 595 nm, respectively.

5.2. Temperature distribution

Fig. 3(a–c) shows a 3D simulation of the temperature profile in skin tissue layers and hair after 50 ms of laser irradiation with a laser fluence of 5 J/cm^2 at 595 nm, 800 nm, and 1064 nm. The amount of laser energy absorbed by skin varies according to wavelength. After absorbing laser energy, it is converted into thermal energy. As shown in Fig. 3(a–c), a large amount of absorbed energy in the epidermis leads to the high surface temperature of the skin. The highest temperature occurred in the laser projection region's center (the hair's tip). The maximum temperature values at laser irradiation at 50 ms at 595 nm, 800 nm, and 1064 nm are 107.8440 °C, 82.3995 °C, and 86.9154 °C, respectively. To see the contour clearly, we have enlarged the image as shown in Fig. 5(a–c). Although the laser intensity of 595 nm and 800 nm in epidermis tissue is very close as shown in Fig. 7 (a), it is clearly seen that the temperature that

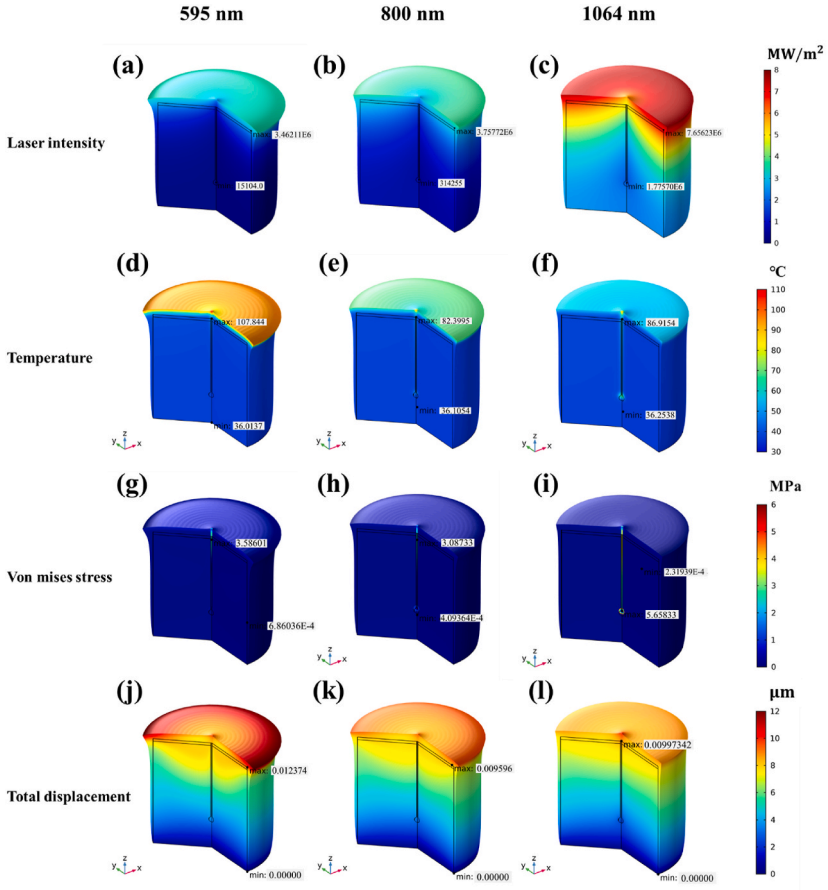

Fig. 3. The 3D laser intensity (a–c), temperature (d–f), Von Mises stress (g–i) and displacement distribution (j–i) at wavelengths of 595 nm, 800 nm, and 1064 nm, laser fluence of 5 J/cm^2 at irradiation time 50 ms.

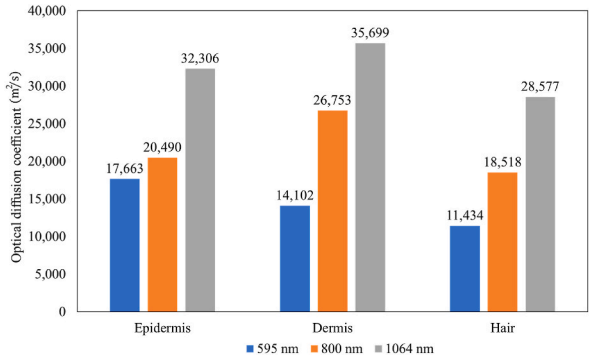

Fig. 4. Comparison of the optical diffusion coefficient of skin tissues at 595 nm, 800 nm, 1064 nm.

occurred is quite different. Including the case of 1064 nm, which has the most significant intensity of laser depositing in epidermis tissue, delivered the lowest temperature. The results show that a wavelength of 595 nm produced the highest surface temperature (epidermis), followed by 800 nm and 1064 nm, respectively. The absorption coefficients of skin tissues such as the epidermis, dermis, and hair vary with each wavelength. It can be clearly seen in the case of 595 nm that the laser deposition within epidermis tissue is the smallest but produces the highest temperature. The optical absorptivity of epidermal tissue at a wavelength of 595 nm is higher than 800 nm and 1064 nm, resulting in higher temperatures on the surface, as evidenced by the absorption coefficient in Table 1.

In Fig. 3(d–f), although the laser irradiation of 595 nm induced the highest temperature on the skin surface, the increase in temperature within the hair and hair follicles was not as effective. It can be seen in Fig. 3 (b-c) that the temperature of hair and hair follicles will be grander when exposed to longer wavelengths. Specifically, in the case of 1064 nm, hair follicle temperature is greater than at other wavelengths. The optical diffusion coefficient impacts deep targeted tissue which in this case is hair follicles, receiving light energy and converting it to heat energy resulting in the maximum temperature occurring in hair follicles, even though the optical absorption coefficient is less than 595 and 800 nm. The hair follicle's temperature dropped when the wavelength decreased by 800 nm and 595 nm, respectively, as related to Fig. 5, which presents the temperature changes at laser irradiation 0–50 ms at the hair tip and hair root after treatment with wavelengths of 595 nm,800 nm, and 1064 nm. The temperature of hair tips is always significantly greater than hair roots. After irradiation, the temperature of hair tips increases rapidly in all cases. In the case of 1064 nm, the temperature of root hair rises gradually, whereas, in the case of 800 nm, it rises slightly. While temperature barely rises in the case of 595 nm.

Fig. 7(c) and (d) depict the temperature distribution of skin tissue along the radial (r-axis and $z = 0$ mm) and longitudinal (z-axis and $r = 0$ mm) axes of different wavelengths at an irradiation time of 50 ms, respectively. Due to the higher absorption coefficient of hair, the center of laser irradiation (hair) is the highest temperature for all wavelengths. Nevertheless, it can be observed that the surface temperature of the skin tissue exceeds 43 °C which is thermal sensitivity (the stimulus temperature of heat pain) in all cases, which may result in the undesired heating of the skin tissue, resulting in thermal injury later. In Fig. 6(b), the potential of 1064 nm to produce heat at the center of the hair follicle ($z = 3$ mm) is greater than that of 595 nm and 800 nm, which is in good agreement with the previous discussions. Moreover, heating by laser irradiation does not have an effect on the temperature of tissue located beneath the hair follicle in the dermis. Fig. 6 depicts the insertion of the temperature line within hair follicles ($z = 3$ mm and $0 \leq r \leq 0.3$ mm) (e). The average temperature inside hair follicles ($z = 3$ mm and $0 \leq r \leq 0.1$ mm) at 595 nm, 800 nm, and 1064 nm wavelengths. It is 36.52 °C, 42.92 °C, and 60.99 °C, respectively. Even though 1064 nm has the highest hair removal efficiency, the average temperature is still below the target temperature of 65 °C. However, we observed that thermal damage could cause injury to the surrounding tissue (dermis), particularly at 1064 nm. It is due to the temperature difference between hair follicles and dermis tissue, which results in heat diffusion ($r > 0.1$) nm. Consequently, using a higher fluence rate may also cause thermal damage to healthy tissue around hair follicles in the form of unwanted heat and it indicates that applying a laser of 1064 nm for therapy is better efficient than in the context of hair

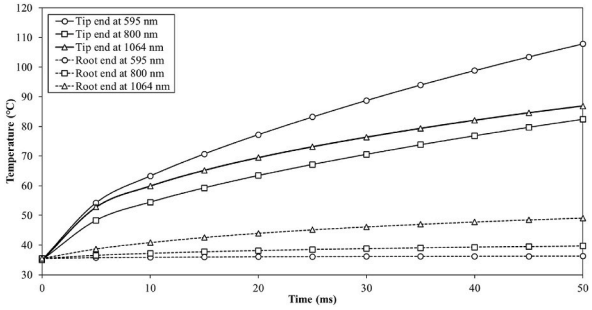

Fig. 5. The temperature changes at laser irradiation 0–50 ms at hair tip and hair root after treatment with wavelengths of 595 nm,800 nm, and 1064 nm.

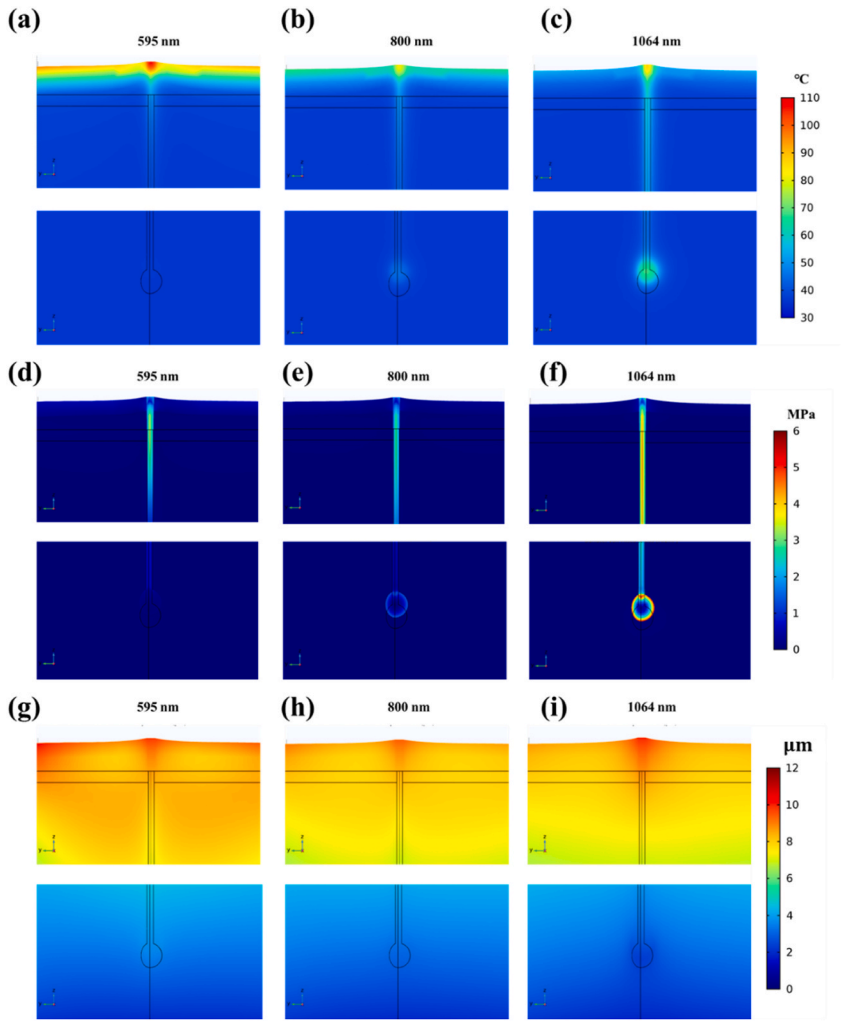

Fig. 6. The 2D model of temperature (a–c), Von Mises stress (d–f) and the displacement distribution (g–i) at wavelengths of 595 nm, 800 nm and 1064 nm, laser fluence of 5 J/cm^2 at irradiation time 50 ms.

removal. The simulation results from the present model were consistent with previously explained research [15,18].

5.3. *The Von Mises stress distribution*

During laser hair removal, temperature gradients within the tissue caused a non-uniform thermal strain with skin tissue, resulting in a mechanical response such as stress within skin tissue. The stress occurred inside the skin tissue is considered as the one of essential parameter due to the skin can response to pain sensation from mechanical stress. Few works have been systematically discussed on this point in the past.

Fig. 3(g–f) and Fig. 6(d–f) present 3D models of Von Mises distribution in skin tissue layers and hair follicles after laser irradiation at 595 nm, 800 nm, and 1064 nm. From the simulation, the maximum stresses are 3.58601 MPa, 3.08733 MPa, and 5.65833 MPa, respectively. In all cases, the highest values are observed in hair tissue. It is because influence of heat of laser energy to thermal strain of tissue. More significant temperature increases in hair increase thermal strain resulting in a high stress value within hair tissue. In addition, Young's modulus of hair is extremely high when compared to other tissues. However, we should concentrate on the epidermis and dermis, healthy tissues capable of responding to pain from mechanical sensations. As mentioned earlier, The lowest value of mechanical sensitivity leading to mechanical pain is 0.2 MPa [7]. Fig. 6(c) depicts the Von Mises stress distribution along the radial direction (r-axis and z = 0 mm) after 50 ms of irradiation time. We observed that the stress also occurred on the surface, reaching the minimum value of mechanical sensitivity, especially in the case of 595 nm and 800 nm. We also observed that the trend of stress lines is agreeable to the temperature lines as shown in Fig. 7 (c). It means that using 595 nm and 800 nm for treatment could result in mechanical pain sensations due to the stress value reaching the minimum of mechanical sensitivity 0.2 MPa (red line). In contrast, the stress is lower in a case of 1064 nm, which means that the patient will not experience mechanical pain during therapy. Instead, the patient may only feel pain due to thermal sensation. The temperature distribution is significantly related to the stress occurring within

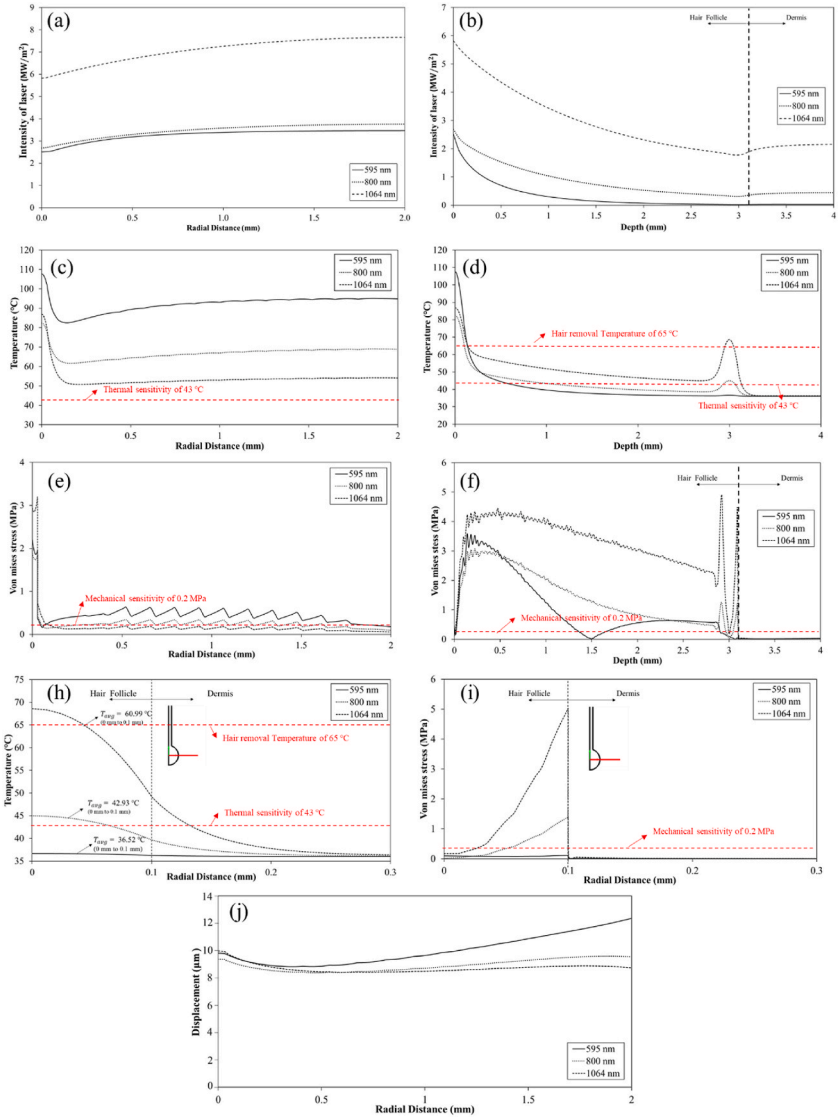

Fig. 7. (a–b) Laser intensity distribution along the radial direction and longitudinal direction (a–b) Temperature distribution along the radial direction and longitudinal direction, (c–d) Von Mises stress distribution along the radial direction and longitudinal direction, (e) comparison of the temperature of hair follicles, (f) comparison of Von Mises stresses of the hair follicle, (g) Total displacement along the radial direction, and all are illustrated at laser fluence of 5 J/cm^2 of 50 ms of irradiation time at wavelength of 595 nm, 800 nm, and 1064 nm.

the skin tissue.

Fig. 6(d) presents the Von Mises stress distribution along the longitudinal direction (z-axis and r = 0 mm) after 50 ms of irradiation time. It has been demonstrated that the stress arises in every instance along the length of the hair tissue. In the case of 1064 nm, the maximum stress at the hair tip decreases gradually along the longitudinal direction then it immediately rises at the hair follicles The same trend can be found in the case of 800 nm as well, but more slightly increased value, which is agree well to the laser intensity and temperature distribution as shown in Fig. 7 (b),(d). While the case of 595 nm is no stress in the hair follicles. In addition, we investigate the Von Mises stress distribution within hair follicles and the surrounding tissue by inserting lines at specific distances (z = 3 mm and 0 $\leq$ r $\leq$ 0.3 mm), as shown in Fig. 7 (i). It indicates that there is no mechanical stress around the hair follicles. we also observed that the stress does not occur in the dermis tissue in all cases. It is no heat production, directing to a temperature that does not rise as well as mechanical stress.

The simulation results indicate that the severity of the physiological effects and mechanical deformation that small temperature increases will increase in sensitive organs such as skin tissue. For effective treatment, it is recommended to use a model that includes mechanical deforamtion to represent the actual behavior of tissue during laser hair removal and related therapy.

5.4. The total displacement distribution

The Von-Mises stress distribution is determined by the thermal expansion of skin tissue caused by the absorption of laser energy. Simultaneously, the displacement distribution of skin tissue also takes place. The effect of laser irradiation of wavelengths 595 nm, 800 nm, and 1064 nm is shown in Fig. 3(j–l) and Fig. 6(g–i). It shows the total displacement distribution of skin tissue layers and hair after 50 ms of laser irradiation with a laser fluence of 5 J/ cm^2 at wavelengths of 595 nm,800 nm, and 1064 nm. The simulation results revealed that the maximum displacement value occurred at the tissue's uppermost surface due to high temperature. Then, it decreases gradually in the direction of depth in all cases. In addition, we also present the total displacement along the radial direction (r-axis and $z = 0$) after 50 ms of laser irradiation at wavelengths of 595 nm, 800 nm, and 1064 nm, as shown in Fig. 6 (g). Laser irradiation at 595 nm produced the most significant total displacement, followed by 800 nm and 1064 nm, respectively. The effect of temperature distribution induced by laser irradiation led to thermal expansion, which was observed clearly in the case of 595 nm, where the values of temperature and Von Mises stress are the highest at the skin's surface. During the therapy process, the temperature has a direct effect on the displacement of the skin. The laser's wavelength has a massive impact on the displacement of skin tissue. The shorter wavelength led to a greater displacement than the longer wavelength.

6. Conclusion

This study presents the photo-thermo-mechanical model coupling the light transport equation, bioheat transfer, and mechanical deformation in order to predict thermal and mechanical response. Systematically, the laser intensity, temperature, Von-Mises stress, and displacement were investigated. As shown in Fig. 2(a–d), the present model was in good agreement with the simulation and experimental results results obtained by Pual et al. [23], including the numerical results obtained by Zhang et al. [44]. Key findings that occurred from this study:

The wavelength of the laser has affected to the optical diffusion coefficient which results in the amount of laser deposition within skin tissue. The hair follicles better receive the laser energy when treated with 1064 nm, followed by 800 nm, and 595 nm, respectively.

The high-temperature area produces a high mechanical stress distribution with skin tissue during therapy as well as the displacement distribution.

In all wavelengths, the temperature at the skin's surface exceeds 43 °C, meaning that the patient or client will experience thermal pain. However, treating with 595 nm and 800 nm may cause mechanical pain in patients, as the stress values are close to the mechanical sensitivity threshold of 0.2 MPa during laser hair removal.

This mathematical model predicts skin tissue's laser intensity, temperature and mechanical deformation during laser hair removal. The performance of laser hair removal was systematically investigated. It is observed that applying different laser wavelengths during laser hair removal results in a very localized increase in skin tissue temperature. It was discovered that using laser wavelengths 595 nm and 800 nm resulted in over-temperature in epidermis tissue and ineffective hair removal.

In contrast, applying a laser of 1064 nm demonstrated the highest efficacy for hair removal. It is evident that the target tissue, the hair follicle, experienced a greater increase in temperature than other tissues. Additionally, the surface temperature of skin tissue is observed to be lower. However, the skin's surface temperature was also high enough to cause thermal injury and pain during laser hair removal in all cases. The obtained temperature profile in skin tissue is utilized as input data for mechanical analysis. It was discovered that when a laser with a different wavelength is applied, Von Mises stress is also so different. In addition, It was found the relationship between temperature and Von Mises stress. The rise in temperature within dermal tissues increases Von Mises stress levels during laser irradiation, particularly in hair. The greatest amount of Von Mises stress values occurred in hair. It is because hair has the highest value of Young's modulus. However, the Von Mises stress distribution along the surface area was greater than the skin's mechanical sensitivity value. Moreover, it was discovered that the skin's displacement was also affected by temperature. Increasing skin temperature had a direct effect on the total displacement. The magnitude of skin surface temperature is anticipated to influence the deformation of skin tissue and the pain.

According to the results, it should consider increasing a laser fluence level for better hair removal in a case of 1064 nm. Applying a 595 nm and 800 nm laser might be appropriate for other medical applications. In addition, it might consider unwanted heating prevention by employing cooling equipment such as Gel, Cooling air, Etc. for higher safety. Hence, suitable therapeutic planning is essential for highly effective treatment outcomes as well as safety standards.

Nevertheless, the current model has some limitations because using the light transport equation to analyze the accumulation of laser energy in tissues. The calculation parameters, such as the refractive index and anisotropy, are required, which differ from Beer-Lambert's law, including the thermal expansion coefficient of tissue affecting the simulation result. In addition, this model was created using 2D asymmetric. It may not be appropriate to add organs or tissues such as blood vessels or tumors, and one should be careful.

This research is a case study for modeling for treatment prediction of laser hair removal that considers mechanical deformation. A comprehensive investigation of physical phenomena that might occur within tissue during therapy is essential, such as in this study focused on predicting temperature and Von Mises stress distribution, which can be used as a guideline for treatment preparation. However, mechanical effects and other physical phenomena should be investigated more clearly,e.g., moisture loss effects (blood and water evaporation) on absorption coefficient, temperature, mechanical stress, and deformation shape changing after laser treatment, including considering dermal tissue as a porous media. Previously mentioned phenomena may directly affect final results, which is the cause of inaccurate pre-diagnosis.

In the medical field, electromagnetic waves, microwave, infrared, laser, and other similar technologies have been utilized to produce thermotherapy treatments for biological tissue such as liver, breast, cardiac, prostate, Etc. The mathematical model of tissue necessitates extensive study. The proposed mathematical model is adaptable to thermotherapy application and development. The

preceding section's simulation results help the field comprehend how to accurately assess tissue temperature and stress during thermotherapy in various treatment situations. This research will help evaluate the trend of laser irradiation on biological tissue and predict therapeutic response. Alternately, in the context of numerical modeling research, the proposed model can be helpful for modeling-interested researchers, who can adapt it for use in medical simulation or related medical applications.

Author statement

Vannakorn Mongkol: *Conceptualization, Methodology, Writing, Software and Validation*. Wutipong Preechaphonkul: *Editing*, Phadungsak Rattanadecho: *corresponding author, Conceptualization, and supervision.* Phadungsak Rattanadecho.

Declaration of competing interest

The authors declare that they have no known competing financial interests or personal relationships that could have appeared to influence the work reported in this paper.

Data availability

Data will be made available on request.

Acknowledgement

This research project is supported by National Research Council of Thailand (NRCT): (Contact No.N41A640213), Research and Innovation, NXPO (Grant number B05F630092, B05F640205), National Research Council of Thailand (Grant No. N42A650197) and the Thailand Science Research and Innovation Fundamental Fund (Grant No. 66082).

References

[1] R.A. Massey, G. Marrero, M. Goel-Bansal, R. Gmyrek, B.E. Katz, Lasers in dermatology: a review, Cutis 67 (6) (2001) 477–484.
[2] M.H. Gold, Lasers and light sources for the removal of unwanted hair, Clin. Dermatol. 25 (5) (2007) 443–453, https://doi.org/10.1016/j.clindermatol.2007.05.017.
[3] R.M. Lavker, S. Miller, C. Wilson, G. Cotsarelis, Z.G. Wei, J.S. Yang, T.T. Sun, Hair follicle stem cells: their location, role in hair cycle, and involvement in skin tumor formation, J. Invest. Dermatol. 101 (1 Suppl) (1993) 16S–26S, https://doi.org/10.1111/1523-1747.ep12362556.
[4] D.T. Gault, A.O. Grobbelaar, R. Grover, S.H. Liew, B. Philp, R.M. Clement, M.N. Kiernan, The removal of unwanted hair using a ruby laser, Br. J. Plast. Surg. 52 (3) (1999) 173–177, https://doi.org/10.1054/bjps.1999.3083.
[5] R.R. Anderson, J.A. Parrish, Selective photothermolysis: precise microsurgery by selective absorption of pulsed radiation, Science (New York, N.Y.) 220 (4596) (1983) 524–527, https://doi.org/10.1126/science.6836297.
[6] F. Xu, T. Lu, Introduction of skin biothermomechanics, in: Introduction to Skin Biothermomechanics and Thermal Pain, Springer, Berlin, Heidelberg, 2011, https://doi.org/10.1007/978-3-642-13202-5_8.
[7] E.W. McCleskey, M.S. Gold, Ion channels of nociception, Annu. Rev. Physiol. 61 (1999) 835–856, https://doi.org/10.1146/annurev.physiol.61.1.835.
[8] L. Carroll, T.R. Humphreys, Laser–tissue interactions, Clin. Dermatol. 24 (1) (2006) 2–7. https://doi:10.1016/j.clindermatol.2005.10.019.
[9] F.W. Neukam, F. Stelzle, Laser tumor treatment in oral and maxillofacial surgery, Phys. Procedia 5 (2010) 91–100, 2010.
[10] D.J. Goldberg, S. Silapunt, Hair removal using a long-pulsed Nd:YAG Laser: comparison at fluences of 50, 80, and 100 J/cm. Dermatologic surgery, official publication for American Society for Dermatologic Surgery [et al 27 (5) (2001) 434–436, https://doi.org/10.1046/j.1524-4725.2001.00329.x.
[11] D.Y. Paithankar, E.V. Ross, B.A. Saleh, M.A. Blair, B.S. Graham, Acne treatment with a 1,450 nm wavelength laser and cryogen spray cooling, Laser Surg. Med. 31 (2) (2002) 106–114, https://doi.org/10.1002/lsm.10086.
[12] E.J. Fiskerstrand, L.O. Svaasand, J.S. Nelson, Hair removal with long pulsed diode lasers: a comparison between two systems with different pulse structures, Laser Surg. Med. 32 (5) (2003) 399–404, https://doi.org/10.1002/lsm.10175.
[13] L.O. Svaasand, J.S. Nelson, On the physics of laser-induced selective photothermolysis of hair follicles: influence of wavelength, pulse duration, and epidermal cooling, J. Biomed. Opt. 9 (2) (2004) 353–361, https://doi.org/10.1117/1.1646174.
[14] P. Babilas, G. Shafirstein, J. Baier, V. Schacht, R.M. Szeimies, M. Landthaler, W. Bäumler, C. Abels, Photothermolysis of blood vessels using indocyanine green and pulsed diode laser irradiation in the dorsal skinfold chamber model, Laser Surg. Med. 39 (4) (2007) 341–352, https://doi.org/10.1002/lsm.20483.
[15] F. Sun, A. Chaney, R. Anderson, G. Aguilar, Thermal modeling and experimental validation of human hair and skin heated by broadband light, Laser Surg. Med. 41 (2) (2009) 161–169, https://doi.org/10.1002/lsm.20743.
[16] L. Ataie-Fashtami, A. Shirkavand, S. Sarkar, M. Alinaghizadeh, M. Hejazi, M. Fateh, H. Mohammadreza, Simulation of heat distribution and thermal damage patterns of diode hair-removal lasers: an applicable method for optimizing treatment parameters, Photomedicine and laser surgery 29 (7) (2011) 509–515.
[17] A. Shirkavand, L. Ataie-Fashtami, S. Sarkar, M.R. Alinaghizadeh, M. Fateh, N. Zand, G.E. Djavid, Thermal damage patterns of diode hair-removal lasers according to various skin types and hair densities and colors: a simulation study, Photomedicine and laser surgery 30 (7) (2012) 374–380, https://doi.org/10.1089/pho.2011.3152.
[18] T.H. Kim, G.W. Lee, J.I. Youn, A comparison of temperature profile depending on skin types for laser hair removal therapy, Laser Med. Sci. 29 (6) (2014) 1829–1837, https://doi.org/10.1007/s10103-014-1584-6.
[19] G.V. Mármol, J. Villena, New 3D in silico model of hair and skin heating during laser hair removal, Res. J. Pharm. Med. Sci 3 (2019) 15–24.
[20] M. Jaunich, S. Raje, K. Kim, K. Mitra, Z. Guo, Bio-heat transfer analysis during short pulse laser irradiation of tissues, Int. J. Heat Mass Tran. 51 (23–24) (2008) 5511–5521.
[21] A. Bhowmik, R. Repaka, S.C. Mishra, K. Mitra, Thermal assessment of ablation limit of subsurface tumor during focused ultrasound and laser heating, J. Therm. Sci. Eng. Appl. 8 (1) (2015).
[22] S.L. Lee, Y.H. Lu, Modeling of bioheat equation for skin and a preliminary study on a noninvasive diagnostic method for skin burn wounds, Burns : journal of the International Society for Burn Injuries 40 (5) (2014) 930–939, https://doi.org/10.1016/j.burns.2013.10.013.
[23] A. Paul, A. Paul, Thermomechanical analysis of a triple layered skin structure in presence of nanoparticle embedding multi-level blood vessels, Int. J. Heat Mass Tran. 148 (2019), 119076, https://doi.org/10.1016/j.ijheatmasstransfer.
[24] R. Dua, S. Chakraborty, A novel modeling and simulation technique of photo–thermal interactions between lasers and living biological tissues undergoing multiple changes in phase, Comput. Biol. Med. 35 (5) (2005) 447–462, https://doi.org/10.1016/j.compbiomed.2004.02.005.
[25] P. Wongchadakul, P. Rattanadecho, Implementation of a 3D thermomechanical model to simulate selection laser heating (effects of wavelength, laser irradiation intensity, and irradiation beam, Area" International Journal of Thermal Sciences 134 (2018) 321–336.

[26] P. Wongchadakul, P. Rattanadecho, T. Wessapan, Simulation of temperature distribution in different human skin types exposed to laser irradiation with different wavelengths and laser irradiation intensities, Songklanakarin J. Sci. Technol. 41 (3) (2019).
[27] P. Wongchadakul, P. Rattanadecho, Mathematical modeling of multilayered skin with embedded tumor through combining laser ablation and nanoparticles: effects of laser beam area, wavelength, intensity, tumor absorption coefficient and its position, Journal homepage 39 (1) (2021) 89–100, https://doi.org/10.18280/ijht.390109.
[28] H.H. Pennes, Analysis of tissue and arterial blood temperatures in the resting human forearm (reprint of 1948 article), J. Appl. Physiol. 85 (1998) 5–34, https://doi.org/10.1152/jappl.1948.1.2.93.
[29] T. Wessapan, S. Srisawatdhisukul, P. Rattanadecho, Numerical analysis of specific absorption rate and heat transfer in the human body exposed to leakage electromagnetic field at 915 MHz and 2450 MHz, J. Heat Tran. 133 (5) (2011).
[30] T. Wessapan, P. Rattanadecho, Numerical analysis of specific absorption rate and heat transfer in human head subjected to mobile phone radiation: effects of user age and radiated power, J. Heat Tran. 134 (12) (2012), https://doi.org/10.1115/1.4006595.
[31] T. Wessapan, P. Rattanadecho, Specific Absorption Rate and Temperature Increase in Human Eye Subjected to Electromagnetic Fields at 900 MHz, 2012.
[32] H.J. Laubach, I.R. Makin, P.G. Barthe, M.H. Slayton, D. Manstein, Intense focused ultrasound: evaluation of a new treatment modality for precise microcoagulation within the skin, Dermatol. Surg. 34 (5) (2008) 727–734, https://doi.org/10.1111/j.1524-4725.2008.34196.x, official publication for American Society for Dermatologic Surgery [et al.
[33] C.H. Li, S.A. Li, Z.H. Huang, W.B. Xu, Skin thermal effect by FE simulation and experiment of laser ultrasonics, in: Applied Mechanics and Materials, Trans Tech Publications, Ltd, 2010, pp. 281–286. https://doi.org/10.4028/www.scientific.net/amm.24-25.281, 24–25.
[34] P. Montienthong, P. Rattanadecho, Focused ultrasound ablation for the treatment of patients with localized deformed breast cancer: computer simulation, ASME. J. Heat Transfer. October 141 (10) (2019), 101101, https://doi.org/10.1115/1.4044393, 2019.
[35] D. Bhargava, P. Rattanadecho, T. Wessapan, The effect of metal objects on the SAR and temperature increase in the human head exposed to dipole antenna (numerical analysis), Case Stud. Therm. Eng. 22 (2020), 100789, https://doi.org/10.1016/j.csite.2020.100789.
[36] W. Preechaphonkul, P. Rattanadecho, The comparative of the performance for predicted thermal models during microwave ablation process using a slot antenna, Case Stud. Therm. Eng. 25 (2021), 100908, https://doi.org/10.1016/j.csite.2021.100908.
[37] Y.C. Fung, Motion, Flow, Stress and Growth. Biomechanics, Springer, 1990 (Verlag).
[38] C. Sherrington, The Integrative Action of the Nervous System Scribner, 1906 (New York).
[39] J.W. Jor, M.P. Nash, P.M. Nielsen, P.J. Hunter, Modelling the mechanical properties of human skin: towards a 3D discrete fibre model, in: 2007 29th Annual International Conference of the IEEE Engineering in Medicine and Biology Society, IEEE, 2007, August, pp. 6640–6643, https://doi.org/10.1109/IEMBS.2007.4353882.
[40] O.R. Garaizar, L. Qiao, N. Anwer, L. Mathieu, Integration of thermal effects into tolerancing using skin model shapes, Procedia Cirp 43 (2016) 196–201, https://doi.org/10.1016/j.procir.2016.02.079.
[41] W.F. Larrabee Jr., A finite element model of skin deformation. I. Biomechanics of skin and soft tissue: a review, Laryngoscope 96 (4) (1986) 399–405, https://doi.org/10.1288/00005537-198604000-00012.
[42] P. Keangin, T. Wessapan, P. Rattanadecho, Analysis of heat transfer in deformed liver cancer modeling treated using a microwave coaxial antenna, Appl. Therm. Eng. 31 (16) (2011) 3243–3254, https://doi.org/10.1016/j.applthermaleng.2011.06.005.
[43] G. Shafirstein, W. Bäumler, M. Lapidoth, S. Ferguson, P.E. North, M. Waner, A new mathematical approach to the diffusion approximation theory for selective photothermolysis modeling and its implication in laser treatment of port-wine stains, Laser Surg. Med.: The Official Journal of the American Society for Laser Medicine and Surgery 34 (4) (2004) 335–347, https://doi.org/10.1002/lsm.20028.
[44] R. Zhang, W. Verkruysse, G. Aguilar, J.S. Nelson, Comparison of diffusion approximation and Monte Carlo based finite element models for simulating thermal responses to laser irradiation in discrete vessels, Phys. Med. Biol. 50 (17) (2005) 4075, https://doi.org/10.1088/0031-9155/50/17/011.
[45] L. Cheung, D. Mitrea, C. Suhrland, H. Zeng, Laser Hair Removal: Comparative Study of Light Wavelength and its Effect on Laser Hair Removal, 2009.
[46] E.V. Ross, Z. Ladin, M. Kreindel, C. Dierickx, Theoretical considerations in laser hair removal, Dermatol. Clin. 17 (2) (1999) 333–355, https://doi.org/10.1016/S0733-8635(05)70091-7.
[47] J. Lepselter, M. Elman, Biological and clinical aspects in laser hair removal, J. Dermatol. Treat. 15 (2) (2004) 72–83.
[48] T.v.(n.d. Kampen, Optical properties of hair, Retrieved, https://pure.tue.nl/ws/files/47042193/632280-1.pdf. (Accessed 21 April 2021).
[49] R. Steiner, D. Russ, W. Falkenstein, A. Kienle, Optimization of laser epilation by simulation of the thermal laser effect, Laser Phys. 11 (1) (2001) 146–153.
[50] S.M. Shapshay, Endoscopic Laser Surgery Handbook (Science and Practice of Surgery Series, No 10), Marcel Dekker Inc, New York, 1987.
[51] F. Xu, T.J. Lu, K.A. Seffen, Biothermomechanics of skin tissues, J. Mech. Phys. Solid. 56 (5) (2008) 1852–1884, https://doi.org/10.1016/j.jmps.2007.11.011.
[52] G. Aguilar, S.H. Díaz, E.J. Lavernia, J.S. Nelson, Cryogen spray cooling efficiency: improvement of port wine stain laser therapy through multiple-intermittent cryogen spurts and laser pulses, Laser Surg. Med.: The Official Journal of the American Society for Laser Medicine and Surgery 31 (1) (2002) 27–35, https://doi.org/10.1002/lsm.10076.
[53] F. Xu, T. Wen, K. Seffen, T. Lu, Modeling of skin thermal pain: a preliminary study, Appl. Math. Comput. 205 (1) (2008) 37–46, https://doi.org/10.1016/j.amc.2008.05.045.
[54] A. Delalleau, G. Josse, J.M. Lagarde, H. Zahouani, J.M. Bergheau, Characterization of the mechanical properties of skin by inverse analysis combined with the indentation test, J. Biomech. 39 (9) (2006) 1603–1610, https://doi.org/10.1016/j.jbiomech.2005.05.001.
[55] F.M. Hendriks, D. Brokken, C.W.J. Oomens, D.L. Bader, F.P.T. Baaijens, The relative contributions of different skin layers to the mechanical behavior of human skin in vivo using suction experiments, Med. Eng. Phys. 28 (3) (2006) 259–266, https://doi.org/10.1016/j.medengphy.2005.07.001.
[56] Y. Yu, W. Yang, B. Wang, M.A. Meyers, Structure and mechanical behavior of human hair, Mater. Sci. Eng. C 73 (2017) 152–163, https://doi.org/10.1016/j.msec.2016.12.008.